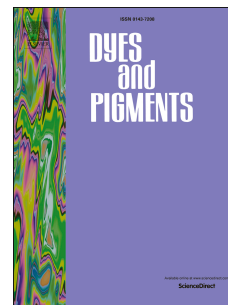


Accepted Manuscript

Novel D-A-D type dyes based on BODIPY platform for solution processed organic solar cells

Junxu Liao, Hongbin Zhao, Yongjun Xu, Zhuodi Cai, Zaixi Peng, Wentao Zhang, Weinan Zhou, Bohong Li, Qiao Zong, Xiaoxi Yang



PII: S0143-7208(16)00031-0

DOI: [10.1016/j.dyepig.2016.01.020](https://doi.org/10.1016/j.dyepig.2016.01.020)

Reference: DYPI 5073

To appear in: *Dyes and Pigments*

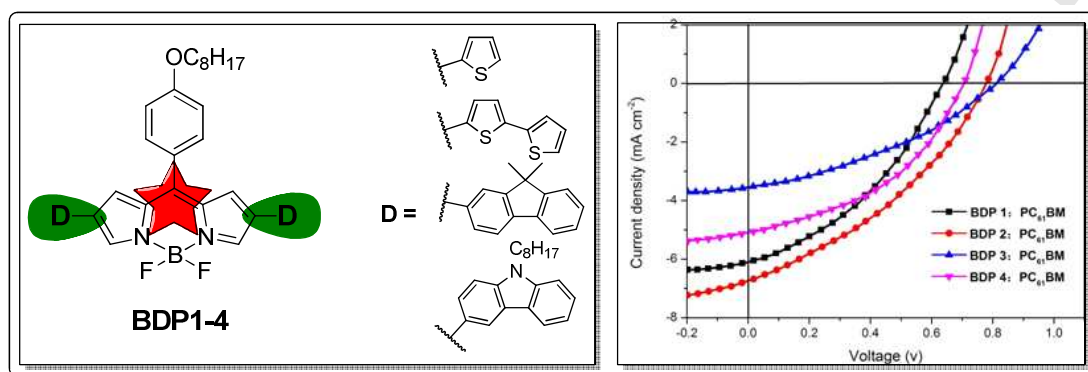
Received Date: 25 November 2015

Revised Date: 18 January 2016

Accepted Date: 23 January 2016

Please cite this article as: Liao J, Zhao H, Xu Y, Cai Z, Peng Z, Zhang W, Zhou W, Li B, Zong Q, Yang X, Novel D-A-D type dyes based on BODIPY platform for solution processed organic solar cells, *Dyes and Pigments* (2016), doi: 10.1016/j.dyepig.2016.01.020.

This is a PDF file of an unedited manuscript that has been accepted for publication. As a service to our customers we are providing this early version of the manuscript. The manuscript will undergo copyediting, typesetting, and review of the resulting proof before it is published in its final form. Please note that during the production process errors may be discovered which could affect the content, and all legal disclaimers that apply to the journal pertain.



Novel D-A-D type dyes based on BODIPY platform for solution processed organic solar cells

Junxu Liao^a, Hongbin Zhao^{b,*}, Yongjun Xu^{b,*}, Zhuodi Cai^c, Zaixi Peng^b, Wentao Zhang^b,
Weinan Zhou^b, Bohong Li^b, Qiao Zong^b, Xiaoxi Yang^{a,b}

^a School of Chemistry and Chemical Engineering, South China University of Technology, Guangzhou 510641,
People's Republic of China

^b College of Energy and Chemical Engineering, Dongguan University of Technology, Dongguan 523808, People's
Republic of China.

^c Chemical Industry and Engineering Society of Dongguan, Dongguan, 523808

Abstract

Four novel symmetrical donor-acceptor-donor (D-A-D) type boron dipyrromethene (BODIPY) based dyes, namely **BDP1-4**, featuring an electron-withdrawing BODIPY motif as the central core, and several types of electron-donating segments, including thiophene, bithiophene, fluorene and carbazole, flanked at its 2,6-positions as terminal groups were synthesized and characterized. All of these **BDPs** exhibit panchromatic absorption covering the wavelength range 300-900 nm with high extinction coefficients (0.78×10^5 - $1.22 \times 10^5 \text{ cm}^{-1} \text{ M}^{-1}$) and relatively lower HOMO energy levels from -5.17 to -5.48 eV. Furthermore, **BDP1-4** show good thermal stabilities, excellent film-forming abilities and low fluorescent quantum yields. **BDP2** flanking with bithiophene units demonstrates superior charge transport property and favorable nanoscale morphology relative to **BDP1**, **BDP3** and **BDP4**. The power conversion efficiency (PCE) values of the organic solar cells

* Corresponding author. Tel.: +86-769-2286-1233; fax: +86-769-2286-1233; e-mail: zhaohbhanlf@163.com.

* Corresponding author. Tel.: +86-769-2286-2605; fax: +86-769-2286-2605; e-mail: hnllxyj@126.com.

(OSCs) based on the **BDPs**/PC₆₁BM (1:0.5, w/w) are 1.49% for **BDP1**, 2.15% for **BDP2**, 1.06% for **BDP3** and 1.56% for **BDP4**, respectively.

Keywords: BODIPY dyes, organic solar cells, donor-acceptor-donor, optoelectronic properties, DFT calculations, photovoltaic performances

Introduction

Organic solar cells (OSCs) are booming as one of the promising technologies for mitigation of the energy crisis because of their potential low-cost fabrication, lightweight, color-tunable feature, and mechanical flexibility [1-4]. Solution processed small molecule organic solar cells have attracted more and more attention benefited from their definite molecular weight, easy purification, and well-reproducible device performances [5-10]. For the traditional fullerene based organic solar cell, the visible and near-infrared solar photons are normally absorbed by the blended donor material because the fullerene acceptor, typically, PC₆₁BM or PC₇₁BM absorbs the solar photons at the near-ultraviolet and visible range. In the solar spectrum ca. 50% of solar photons is located in the wavelength of 600–1000 nm and the highest photon flux of the solar spectrum is distributed around 600–800 nm [11]. Therefore, designing narrow-band gap (< 1.6 eV, or with onset absorption beyond 800 nm) small-molecule donors are required in the field of small-molecule organic solar cells.

Boron dipyrromethene (BODIPY) dyes have attracted considerable interest in recent years owing to a unique combination of facile synthesis, stability, high absorption coefficient, and high photoluminescence efficiency [12-16], along with the spectroscopic and photophysical properties of BODIPYs can be fine-tuned by attachment of ancillary residues at the appropriate positions of

the BODIPY core [17-18]. The BODIPY derivatives commonly possess solution-state absorption spectra with absorption maxima exceeding 500 nm, even up to 1000 nm, by a suitable modification [17-21]. In addition, BODIPY inherently bear deep HOMO energy levels (< 5.2 eV) [17]. Therefore, the relatively high extinction coefficient of the BODIPY core combined with deep HOMO energy levels and propensity to π -stack in solid-state, make BODIPY-based materials attractive candidates for organic solar cells [17]. However, to our knowledge, there are only several reports on organic solar cells based on BODIPY to date. Roncali et al. reported the first examples of BODIPY donors involving two styryl units along with PC₆₁BM as the electron acceptor for solution-processed bulk-heterojunction (BHJ) OSCs [22-23]. Subsequently, other groups reported BHJ OSCs based on BODIPY small molecules and polymers [16, 24-34], and the best PCE based on BODIPY small molecules was only 5.05% [35]. Therefore, the development of novel BODIPY based small molecule materials with versatile structures and further obtaining insight into their potential photovoltaic application has aroused our interest.

Inspired by the strategy for constructing low-band gap materials with conjugated donor-acceptor (D-A) system [2], herein, the highly flexible BODIPY platform was selected for the development of D-A structural small molecular-based panchromatic donors. In this contribution, we present four novel D-A-D type BODIPY dyes, **BDP1-4**, consisting of an electron-withdrawing BODIPY as central acceptor, and different electron-donating aromatic groups, including thiophene, bithiophene, fluorine and carbazole, symmetrically flanked at 2,6-positions of BODIPY nucleus as terminal conjugated donors (Scheme 1). We expect that these chromophores would significant broadening of absorption and improving light-harvesting ability in the whole sunlight region. The photophysical properties and electrochemical behaviors of these dyes were studied systematically

to reveal the relationships between the structures and the photoelectric characteristics. Time-dependent density functional theory (TD-DFT) calculations were performed to further understanding their structural and electronic features. Furthermore, the photovoltaic performances of these dyes were investigated in detail to insight their potential OSCs applications.

2. Experimental section

2.1. Materials

2,2'-((4-(octyloxy)phenyl)methylene)bis(1H-pyrrole) (**3**), 5,5-difluoro-10-(4-(octyloxy)phenyl)-5H-dipyrrolo[1,2-c:2',1'-f][1,3,2]diazaborinin-4-ium-5-uide (**4**) and 2,8-dibromo-5,5-difluoro-10-(4-(octyloxy)phenyl)-5H-dipyrrolo[1,2-c:2',1'-f][1,3,2]diazaborinin-4-ium-5-uide (**5**) were prepared following the reported procedures [34, 36-37]. Compound **6**, **7**, **8** and **9** were synthesized according to the literatures [38-40]. THF and toluene were dried and distilled over sodium and benzophenone. DMF, dichloromethane, ethyl acetate were dried under 4A molecular sieves. Pyrrole was distilled from CaH₂ before use. All other reagents and chemicals were purchased from commercial sources (Aldrich, TCI, J&K) and used without further purification. Column chromatography was performed on silica (300–400 mesh).

2.2. Measurements and characterization

All ¹H and ¹³C NMR spectra were recorded on a Bruker Avance spectrometer (600 and 151 MHz, respectively) and a Bruker Avance spectrometer (400 and 101 MHz, respectively) with tetramethylsilane (TMS) as the internal standard. Matrix-assisted laser desorption/ionization time of flight mass spectra (MALDI-TOF-MS) were recorded on Bruker ultraflex-II spectrometer, matrix-assisted laser desorption ionization mass spectrometry using an α -cyano-4-hydroxy-

cinnamic acid (α -CHCA) matrix. High resolution mass spectra (HRMS) were recorded on an Agilent 6530 Accurate Mass Q-TOF LC-MS instrument. Absorption spectra were collected on an SHIMADZU UV-2550 spectrophotometer and emission spectra were recorded by using a Hitachi F-4500 instrument. Excitation and emission spectra were fully corrected by reference to a standard lamp. Cyclic voltammetric (CV) was carried out on a CHI660E electrochemical workstation utilizing the three electrode configuration consisting of a gold electrode (working electrode), platinum wire (auxiliary electrode) and Ag/AgCl electrode (reference electrode). The experiment was performed in dry dichloromethane solution using 0.1 M n-Bu₄NPF₆ as supporting electrolyte. The solution was deoxygenated at room temperature under nitrogen protection. Thermogravimetric analyses (TGA) were conducted under a dry nitrogen gas flow at a heating rate of 20 °C min⁻¹ on a NETZSCH TG 209F3 instrument. Differential scanning calorimetric (DSC) were recorded on a NETZSCH DSC 200F3 instrument. Topographic images of the films were obtained on a Veeco MultiMode atomic force microscopy (AFM) in the tapping mode using an etched silicon cantilever at a nominal load of ~2 nN, and the scanning rate for a 5 μ m \times 5 μ m image size was 1.0 Hz. Quantum chemical calculations for complexes **BDP1-4** were conducted at the DFT level of theory, in conjunction with the B3LYP functional [41] and the 6-31G* basis set [42], as implemented in the Gaussian 09 program package [43].

2.3. Device fabrication and characterization

OSC devices were fabricated using indium tin oxide (ITO) glass as an anode, Ca/Al as a cathode, and a blend film of the **BDPs**/PC₆₁BM as a photosensitive layer. After a 30 nm buffer layer of poly(3,4-ethylenedioxy-thiophene) and polystyrene sulfonic acid (PEDOT:PSS) was spin-coated onto the precleaned ITO substrate, the photosensitive layer was subsequently prepared

by spin coating a solution of the **BDPs**/PC₆₁BM (1:0.5, w/w) in CHCl₃ on the PEDOT:PSS layer with a concentration of 25 mg mL⁻¹, and dried under nitrogen at room temperature in a nitrogen-filled glove-box. Ca (10 nm) and Al (100 nm) were successively deposited on the photosensitive layer in vacuum and used as top electrodes. The current density-voltage (*J-V*) characteristics of the devices were carried out on a computer controlled Keithley 236 source measurement system under simulated 100 mW cm⁻² (AM 1.5 G) irradiation from a Newport solar simulator. Light intensity was calibrated with a standard silicon solar cell. The active area was 0.1 cm² for each cell. The thicknesses of the spun-cast films were recorded by a profilometer (Alpha-Step 200, Tencor Instruments). The external quantum efficiency (EQE) was measured by a Stanford Research Systems model SR830 DSP lock-in amplifier coupled with WDG3 monochromator and a 150W xenon lamp.

2.4. Synthesis of target molecules

2.4.1. Synthesis of **BDPI**

Compound **5** (277 mg, 0.5 mmol) was dissolved in toluene (30 mL), followed by addition of tributyl(thiophen-2-yl)stannane **6** (448 mg, 1.2 mmol), Pd(PPh₃)₄ (23 mg, 0.02 mmol). The resulting mixture was refluxed at 110 °C under argon atmosphere for 24 h. Then the reaction mixture was brought to room temperature, washed with brine, and extracted by ethyl acetate. Organic layers were combined, dried over anhydrous Na₂SO₄, filtered, and evaporated to dryness. Purification was performed by column chromatography on silica gel using petroleum ether/ethyl acetate (8:1, v/v) as eluent, from which the desired product **BDPI** was obtained as a dark blue solid (132 mg, yield 47%). mp: 156-158 °C. ¹H NMR (400 MHz, CDCl₃) δ 8.17 (s, 2H), 7.62 (d, *J* = 8.3 Hz, 2H), 7.23 (d, *J* = 4.9 Hz, 2H), 7.18 (d, *J* = 2.8 Hz, 2H), 7.11 (d, *J* = 8.3 Hz, 2H),

7.07–7.02 (m, 2H), 7.01 (s, 2H), 4.10 (t, $J = 6.3$ Hz, 2H), 1.98–1.82 (m, 1H), 1.64–1.19 (m, 12H), 0.98–0.74 (m, 3H). ^{13}C NMR (101 MHz, CDCl_3) δ 162.02, 146.57, 141.00, 136.02, 132.46, 127.96, 127.28, 126.27, 125.87, 124.76, 124.31, 123.29, 114.83, 68.48, 31.78, 31.57, 29.30, 26.10, 25.77, 22.71, 14.16. MALDI-TOF-MS, m/z : calcd for $\text{C}_{31}\text{H}_{31}\text{BF}_2\text{N}_2\text{OS}_2$ $[\text{M}]^+$: 560.194; found 560.198. HRMS, m/z : calcd for $\text{C}_{31}\text{H}_{31}\text{BF}_2\text{N}_2\text{OS}_2$ $[\text{M}]^+$: 560.1939; found 560.1937.

2.4.2. Synthesis of **BDP2**

Compound **BDP2** was synthesized according to the same procedure as for preparing **BDP1** using [2,2'-bithiophen]-5-yltributylstannane **7** as reactant. The crude product was purified on silica column using petroleum ether/ethyl acetate (8:1, v/v) as eluent to give the pure compound **BDP2** as dark blue solid in 52% yield. mp: 172-173 °C. ^1H NMR (400 MHz, CDCl_3) δ 8.18 (s, 2H), 7.62 (d, $J = 8.2$ Hz, 2H), 7.23 (d, $J = 5.0$ Hz, 2H), 7.17 (d, $J = 3.0$ Hz, 2H), 7.11 (t, $J = 7.2$ Hz, 6H), 7.06–7.00 (m, 2H), 6.99 (s, 2H), 4.11 (t, $J = 6.3$ Hz, 2H), 1.87 (d, $J = 14.0$ Hz, 2H), 1.68–1.16 (m, 12H), 0.98–0.75 (m, 3H). ^{13}C NMR (101 MHz, CDCl_3) δ 162.06, 146.21, 140.92, 137.20, 136.26, 135.58, 134.76, 132.51, 127.95, 127.80, 125.85, 124.56, 124.47, 124.07, 124.00, 123.72, 114.86, 68.52, 31.95, 29.75, 29.41, 29.31, 26.04, 22.82, 14.11. MALDI-TOF-MS, m/z : calcd for $\text{C}_{39}\text{H}_{35}\text{BF}_2\text{N}_2\text{OS}_4$ $[\text{M}]^+$: 724.169; found 724.232. HRMS, m/z : calcd for $\text{C}_{39}\text{H}_{35}\text{BF}_2\text{N}_2\text{OS}_4$ $[\text{M}]^+$: 724.1693; found 724.1690.

2.4.3. Synthesis of **BDP3**

To the solution of compound **5** (277 mg, 0.5 mmol) and 2-(9,9-dimethyl-9H-fluoren-2-yl)-4,4,5,5-tetramethyl-1,3,2-dioxaborolane **8** (387 mg, 1.2 mmol) in toluene (20 mL) was added $\text{Pd}(\text{PPh}_3)_4$ (23 mg, 0.02 mmol) and sodium carbonate solution (10 mL, 2 M in water), the mixture was stirred at 90 °C under argon atmosphere for 24 h. Then the reaction mixture was brought to

room temperature, washed with brine, and extracted by ethyl acetate. Organic layers were combined, dried over anhydrous Na_2SO_4 , filtered and evaporated to dryness. The residue was purified by column chromatography on silica gel using petroleum ether/ethyl acetate (6:1, v/v) as eluent, afforded the desired product **BDP3** as dark blue solid (205 mg, yield 41%). mp: 181-182 °C. ^1H NMR (400 MHz, CDCl_3) δ 8.37 (s, 2H), 7.71 (dd, $J = 14.4, 8.0$ Hz, 6H), 7.60 (s, 2H), 7.54 (d, $J = 7.7$ Hz, 2H), 7.45 (d, $J = 6.4$ Hz, 2H), 7.35 (dd, $J = 11.5, 6.1$ Hz, 4H), 7.20 (s, 2H), 7.16 (d, $J = 8.2$ Hz, 2H), 4.13 (t, $J = 6.1$ Hz, 2H), 1.89 (dd, $J = 13.7, 6.7$ Hz, 2H), 1.64–1.15 (m, 12H), 1.02–0.75 (m, 15H). ^{13}C NMR (101 MHz, CDCl_3) δ 161.89, 154.51, 153.83, 146.26, 141.55, 138.74, 135.87, 134.57, 132.64, 131.82, 127.40, 127.11, 126.25, 125.06, 124.57, 122.65, 120.57, 120.03, 119.65, 114.81, 77.37, 76.74, 68.43, 46.99, 31.79, 29.74, 29.40, 29.29, 29.27, 27.29, 26.14, 22.68, 14.15, 1.04. MALDI-TOF-MS, m/z: calcd for $\text{C}_{53}\text{H}_{51}\text{BF}_2\text{N}_2\text{O}$ $[\text{M}]^+$: 780.406, found 780.485. HRMS, m/z: calcd for $\text{C}_{53}\text{H}_{51}\text{BF}_2\text{N}_2\text{O}$ $[\text{M}]^+$: 780.4063, found 780.4059.

2.4.4. Synthesis of **BDP4**

Compound **BDP4** was synthesized according to the same procedure as for preparing **BDP3** using 9-octyl-2-(4,4,5,5-tetramethyl-1,3,2-dioxaborolan-2-yl)-9H-carbazole **9** as reactant. The crude product was purified on silica column using petroleum ether/ethyl acetate (10:1, v/v) as eluent to give the pure compound **BDP4** as dark blue solid in 59% yield. mp: 126-127 °C. ^1H NMR (400 MHz, CDCl_3) δ 8.46 (s, 2H), 8.34 (s, 2H), 8.20 (d, $J = 7.6$ Hz, 2H), 7.79 (d, $J = 8.4$ Hz, 2H), 7.74 (d, $J = 8.4$ Hz, 2H), 7.56 (t, $J = 7.5$ Hz, 2H), 7.48 (d, $J = 8.8$ Hz, 4H), 7.37–7.30 (m, 4H), 7.23 (d, $J = 8.5$ Hz, 2H), 4.38 (t, $J = 7.0$ Hz, 4H), 4.21 (t, $J = 6.4$ Hz, 2H), 2.03–1.88 (m, 6H), 1.70–1.22 (m, 30H), 1.04–0.85 (m, 9H). ^{13}C NMR (101 MHz, CDCl_3) δ 161.74, 145.30, 141.26, 140.97, 139.97, 135.93, 135.04, 132.48, 126.46, 125.98, 124.15, 123.85, 123.55, 123.40, 122.82,

120.51, 119.05, 117.22, 114.70, 109.07, 108.92, 68.49, 43.29, 31.81, 29.73, 29.41, 29.39, 29.29, 29.28, 29.19, 29.02, 27.34, 26.14, 22.71, 22.62, 14.14, 14.07. MALDI-TOF-MS, m/z: calcd for $C_{63}H_{73}BF_2N_4O$ $[M]^+$: 950.585; found 950.769. HRMS, m/z: calcd for $C_{63}H_{73}BF_2N_4O$ $[M]^+$: 950.5845; found 950.5834.

3. Results and discussion

3.1. Synthesis and thermal property

The synthetic routes for the four novel D-A-D type BODIPY dyes are depicted in Scheme 1. For the construction of these dyes, we utilized the Suzuki and Stille cross-coupling reaction to connect two electron-donating moieties covalently to the 2,6-positions of BODIPY nucleus, where a bisbromated BODIPY **5** should be prerequisite for the synthesis. Thus, our synthetic approach started with the preparation of **5** from commercially available 4-hydroxybenzaldehyde **1** through a four-step sequence involving alkylation-condensation-chelation-bisbromination reactions. In particular, alkylation of **1** with 1-bromooctane readily gave **2** in quantitatively. Condensation of **2** with excess pyrrole using $InCl_3$ as catalyst efficiently afforded the desired dipyrromethane **3**. Then, chelating reaction was performed between **3** and $BF_3 \cdot Et_2O$ in the presence of chloranil to give the corresponding BODIPY **4**. Subsequently, bisbromination of **4** with NBS in a mixture of DMF and CH_2Cl_2 solution efficiently provided the key intermediate **5**. Finally, the classical Stille and Suzuki cross-coupling reactions were performed to execute the conversion from **5** to the target BODIPY dyes **BDP1-4**. These **BDPs** exhibit good solubility in common organic solvents such as ethyl acetate, dichloromethane and THF. All these intermediates and the final BODIPY dyes were readily available, and the success in the synthesis of these products was fully characterized by a

range of spectroscopies including ^1H NMR, ^{13}C NMR, MALDI-TOF-MS and HRMS.

TGA and DSC curves provide useful information about the thermostability of these four dyes. The TGA curves of **BDP1-4** are depicted in Fig.1, and the corresponding data are summarized in Table 1. The decomposition temperature (T_d) level of 221 °C for **BDP1**, 305 °C for **BDP2**, 328 °C for **BDP3** and 301 °C for **BDP4** are observed at a 5% weight loss under nitrogen protection, respectively. In DSC, the dyes were heated from 25 to 300 °C and then again cooled to 25 °C with a rate of 10°C/min under nitrogen flow. The chromatograms are shown in Fig S1-Fig S4 (ESI). **BDP1** exhibits an endothermic peak at 157 °C, which indicates the melting temperature of **BDP1**. This melting temperature is approximately consistent with the value (156-158 °C) obtained by melting point meter. Nevertheless, no exothermic peak is observed during the cooling process in DSC curve. Similarly, **BDP2-4** display endothermic peaks at 172 °C, 180 °C and 127 °C, respectively. The results show that all of these **BDPs** have high thermal stability and good enough for the application in optoelectronic devices.

3.2. Electronic absorption

The normalized absorption spectra of these BODIPY dyes **BDP1-4** in dichloromethane solution are depicted in Fig. 2, and the corresponding optical data are summarized in Table 1. As shown in Fig. 2, the absorption spectrum of the reference molecule **4** is characterized by a strong $S_0 \rightarrow S_1$ ($\pi-\pi^*$) transition at 509 nm and a weaker broad band around 420 nm arising from the $S_0 \rightarrow S_2$ ($\pi-\pi^*$) transition. **BDP1**, **BDP2**, **BDP3**, and **BDP4** show broad absorption with three distinct bands in the absorption spectra. The first one at the shorter wavelength region at around 280-350 nm is assigned to localized $\pi-\pi^*$ transition of the electron-rich donors, such as thiophene, bithiophene, fluorene and carbazole moieties. The second one region at around 350-500 nm is attributed to the

$S_0 \rightarrow S_2 (\pi-\pi^*)$ transition of BODIPY core. The third one at the longer wavelength region at around 500-800 nm is ascribed to a mixture of $S_0 \rightarrow S_1 (\pi-\pi^*)$ transition and the intramolecular charge transfer (ICT) transition between electron-rich donors and an electron-deficient acceptor. Compared with reference **4**, the maximum absorption wavelength λ_{\max} is red-shifted by 112 nm for **BDP1**, 169 nm for **BDP2**, 115 nm for **BDP3**, and 146 nm for **BDP4**, which can be assigned to the extended π -conjugation of the backbone. **BDP2** and **BDP4** display more bathochromic shifts than **BDP1** and **BDP3** can be explained as bithiophene and carbazole segments inherently possess stronger electron-donating ability, resulting in more intensive ICT transitions. Fig. 2 also reveals that the absorption spectra of **BDPs** lie in the broad region range of 300–800 nm from the visible to a portion of the NIR region of the solar spectrum, which is a desirable property for generating higher photocurrents in solar cells. The optical band gaps (E_g^{opt} , Table 1) of the four **BDPs** estimated from the UV-vis onset absorptions are 1.71, 1.59, 1.77, and 1.65 eV for **BDP1**, **BDP2**, **BDP3** and **BDP4**, respectively. Noteworthy, all these dyes show high extinction coefficients range from 7.8×10^4 to $1.2 \times 10^5 \text{ cm}^{-1} \text{ M}^{-1}$ in solution, which ensured their excellent light harvesting ability. In comparison with the absorption spectrum in CH_2Cl_2 solution, broader absorption bands with obvious bathochromic shifts and higher coefficients were observed in the solid state (Fig. 3). This could be attributed to the molecular stacking in solid state, which suggests an increased conjugation length in the solid state due to the π - π stacking of the nearly planar conformations of BODIPY. Consequently, these **BDPs** exhibit panchromatic absorption covering the wavelength from 300 nm to 900 nm with extinction high coefficients. Furthermore, all these dyes exhibit perfect solubility and film-forming ability. The desirable combination of attractive photophysical characteristics, good solubility, favorable film-forming ability and functional group tolerance

indicate that these dyes are promising applying in solution processed organic solar cells devices.

3.3. Photoluminescence

The photoluminescence of complexes **BDP1-4** in different solvents were investigated at room temperature. Rhodamine B ($\Phi = 0.71$) was used as standard in methanol to estimate the fluorescence quantum yield [44]. Their normalized emission spectra in CH_2Cl_2 solution at a concentration of 1×10^{-7} mol/L are illustrated in Fig. 4. The emission band maxima and quantum yields are listed in Table 1. Excitation of these compounds at their respective three absorption bands at room temperature resulted in the same near-infrared emissive BODIPY dyes with emission maxima of 671, 748, 668 and 720 nm, respectively. This can be explained on the basis of a photo-induced energy transfer from the BODIPY $\pi\text{-}\pi^*$ excited state to the lower lying singlet excited state of the donor moieties and/or to the existence of new non-radiative pathways from the BODIPY $\pi\text{-}\pi^*$ excited state to the ground state [45]. The results also imply that there is a thorough intermolecular energy transfer of the excitons from the BODIPY core to the donor unit. These BODIPY dyes with donor units at 2,6-positions (**BDP1-4**) present red-shifted emissions compared to the BODIPY **4**, which indicate that the substituents significantly affect the emission and bring forth an effective intramolecular energy transfer for the excitons in the D-A units. The significant Stokes shifts of these dyes are range from 1263 to 1567 cm^{-1} . Taking these features into account, we can assign the observed emission to the ICT emission. Solvent dependence study was performed in solvents with various polarities, such as methanol, dichloromethane, acetone and ethyl acetate (Fig. S5, ESI). The minor solvatochromic affect were observed for **BDP1-4** indicate that these emissions were not caused by solvent effect and/or aggregation effect. Additionally, the excitation spectra of **BDP1-4** are essentially in agreement with their absorption spectra. These results further confirm the ICT

emission nature of these dyes.

On the other hand, **BDP1-4** give low fluorescent quantum yields (Table 1), which could be attributed to the increased internal conversion according to the energy gap law that states the non-radiative deactivation probability of S_0 - S_1 increases as the energy gap of S_0 - S_1 decreases in a highly extended conjugating system. In general, photoluminescence (PL) quenching provides the direct evidence for exciton dissociation, and thus efficient PL quenching is necessary to obtain efficient organic solar cells.

3.4. Electrochemical properties

In order to investigate the electrochemical behaviors of **BDP1-4**, the electronic states of these dyes were studied through cyclic voltammetry in CH_2Cl_2 solution at a scan rate of 100 mVs^{-1} using Bu_4NPF_6 as supporting electrolyte. Potentials were standardized with ferrocene/ferrocenium (Fc/Fc^+) couple as internal reference vs Ag/AgCl . The cyclic voltammograms of **BDP1-4** are illustrated in Fig. 5, and their electrochemical properties are summarized in Table 2. As shown in Fig. 5, dyes **BDP1-4** present onset oxidation potential as 1.15, 0.91, 1.20 and 0.89 V, respectively. It indicates that the aromatic substituents have significant effects on the $E_{\text{onset}}^{\text{ox}}$. The reduction potentials (E_{red}) calculated from $E_{\text{onset}}^{\text{ox}} - E_{\text{g}}$ are approximately matched with the experimental values obtained from reduction waves. The corresponding ionization potential (can be considered as the highest occupied molecular orbital, HOMO, energy level) of **BDP1-4** are calculated (-5.43, -5.19, -5.48 and -5.17 eV, respectively) from the equation $E_{\text{HOMO}} = [-(E_{\text{onset}}^{\text{ox}} - 0.52) - 4.8] \text{ eV}$, where 0.52 V is the value for ferrocene versus Ag/AgCl and 4.8 eV is the energy level of Fc/Fc^+ relative to the vacuum energy level. These dyes are actually located at very low energy levels, which is attractive property in bulk-heterojunction (BHJ) solar cell device. The important factor

for this result is that the strong electron donating group would cause an intensive ICT process. The reduction potential versus NHE (E_{red}), which corresponds to the electron affinity (can be considered as the lowest unoccupied molecular orbital, LUMO, versus NHE) can be obtained from $E_{\text{onset}}^{\text{ox}}$ and E_{g} . The results are shown in Table 2. It should be noted that HOMO/LUMO levels of these dyes are favorable match with the n-type semiconductor such as PCBM, which suggests that they are capable of OSCs applications.

3.5. Theoretical calculations

For a better understanding of the structural and electronic features of these novel dyes, the TD-DFT theoretical calculations were further performed, and the optimized structures and the electronic distribution in HOMO and LUMO levels are presented in Fig. 6 and Fig. 7. All calculations were carried out with the Gaussian 09 program suite by using the B3LYP method and 6-31 G* basis set. From the optimized ground-state geometries of the dyes in Fig. 6, we can see that the dihedral angle between the donor units and the BODIPY framework are computed to be 12.2° for **BDP1**, 3.5° for **BDP2**, 25.7° for **BDP3**, and 22.8° for **BDP4**, respectively. The optimized ground-state geometries indicate that all these dyes exhibit relatively coplanar molecule structures. Generally, the high degree of molecular coplanarity facilitate the effect ICT transition in D-A structural molecule, resulting in bathochromic shifted absorption, which is consistent with the UV-vis absorption spectra observed in solution.

The electron distributions of **BDP1–4** indicate that π -electrons in the HOMO are delocalized over the entire molecule backbone, offering effective orbital interactions among the stacked π -systems, while their LUMOs are mainly localized on the BODIPY moieties. Therefore, the HOMO–LUMO transition that is the dominant contributing configuration to the S_1 state in

BDP1-4 should be ascribed to a mixture of π - π^* and ICT characters, which is consistent with their absorption assignments. On the other hand, the calculated results clearly demonstrate that strong electron-donating substituent with more coplanar geometry, such as dithiophene in **BDP2**, increases the energy level of HOMO more than that of LUMO, thus the HOMO-LUMO gap decreases, causing a bathochromic shift of the π - π^* /ICT band. This trend follows that observed from the UV-vis absorption measurement. Fig. 7 presents the HOMO-LUMO energy differences (energy band gaps, calculated E_g^{cal}) of **BDP1-4**. We can see that the trend of the predicted E_g^{cal} values (1.09–1.43 eV) is in consistent with the estimated E_g^{opt} (calculated from the ground-state absorption, 1.59–1.77 eV) in Table 1.

3.6. Photovoltaic performance

BHJ OSCs were fabricated by solution processed with a general device structure of ITO/PEDOT:PSS/active layer/Ca/Al to investigate the photovoltaic properties. The device fabrication processes are described in detail in the Experimental section. The active layer consisted of the donor of **BDPs** and the acceptor of PC₆₁BM. In this contribution, optimal fabrication conditions were obtained from a CHCl₃ solution with a typical concentration of 25 mg/mL at room temperature. As we known, the performances of OSCs could be strongly affected by the processing parameters, including the **BDPs**/PC₆₁BM ratio (w/w), thicknesses and annealing temperatures of the photoactive layer. In order to understand these parameters influence on the photovoltaic properties, the **BDP1**:PC₆₁BM based devices at different donor-acceptor ratios, as well as thicknesses of the photoactive layer and the annealing temperatures were systematically investigated, and the corresponding data are summarized in Table S1 (ESI). The best performance was achieved with a donor-acceptor ratio of 1:0.5 and the active layer thickness of 110 nm

obtained from a CHCl_3 solution at a total solid concentration of 25 mg/mL under a spin-coating rate of 1500 rpm, followed by annealing at 100 °C for 10 min.

At these optimized conditions, Fig. 8 shows the current density-voltage (J - V) characteristics of these devices using **BDPs** as donor and PC_{61}BM as acceptor, and the corresponding data are listed in Table 3. As a result, a maximal PCE of 1.49% with a V_{oc} of 0.64 V, a J_{sc} of 6.02 mA cm^{-2} and FF of 39% was obtained in the **BDP1** based device. As we expected, the **BDP2** based device demonstrated the highest PCE of 2.15% with a V_{oc} of 0.78 V, a J_{sc} of 6.77 mA cm^{-2} and FF of 41%. The PCE of 1.06% and 1.56% were obtained in the **BDP3** and **BDP4** based devices, respectively. It is obvious that the better performance of the **BDP1**, **BDP2** and **BDP4** based devices relative to **BDP3** based device is mainly contributed by the significantly higher J_{sc} values, which probably cause by their broader absorption in visible and near-infrared range.

The external quantum efficiency (EQE) curves of the devices under the optimized conditions were also investigated. As shown in Fig. 9, the EQE curves for these **BDPs** based devices exhibit very broad wavelength range from 300 nm to nearly 900 nm, which match their absorption assignments. The maximum EQE of 35% at 692 nm is observed in the **BDP2** based device. According to the EQE curves and the solar irradiation spectra, the integral current density of values of OSCs are calculated to be 5.96, 6.63, 3.65 and 5.21 mA cm^{-2} for **BDP1**, **BDP2**, **BDP3** and **BDP4**, respectively, which are in consistent with the values obtained from J - V measurements.

3.7. Hole mobility of the **BDPs** films.

Generally, a high hole mobility is beneficial for efficient hole transport within an active layer without large photocurrent loss caused by recombination with opposite charges. In order to get some ideas about the influence of the chemical structures on their charge transporting properties,

hole mobilities (μ_h) of the hole-only devices were measured by the space-charge limited-current (SCLC) method [46] with a device structure of ITO/PEDOT:PSS/active layer/Au. The SCLC is estimated by the Mott Gurney equation [47]: $J = 9\epsilon_0\epsilon_r\mu_h V^2/8L^3$, in which J is current density, L is film thickness of active layer (85 nm), μ_h is hole mobility, ϵ_r is relative dielectric constant of the transport medium, ϵ_0 is permittivity of free space (8.85×10^{-12} F m⁻¹), V is internal voltage in the device and $V = V_{appl} - V_a - V_{bi}$, where V_{appl} is applied voltage, V_a is voltage drop, and V_{bi} is the built-in voltage due to the relative work function difference of the two electrodes. As depicted in Fig. 10, the hole-only mobilities of these **BDPs** are calculated to be 8.92×10^{-5} cm² V⁻¹ s⁻¹, 6.35×10^{-4} cm² V⁻¹ s⁻¹, 3.11×10^{-5} cm² V⁻¹ s⁻¹ and 6.02×10^{-5} cm² V⁻¹ s⁻¹ in the hole-only **BDPs**/PC₆₁BM based devices, respectively (Table 3). It is obvious that **BDP2** presents relatively higher hole mobility than **BDP1**, **BDP3** and **BDP4**, which is also responsible for the high *FF* of **BDP2** and the better performance of the devices using this molecule. It firmly verifies that rigid molecular structure facilitates the hole mobility.

3.8. Morphologies of the active layers.

Atomic force microscopy (AFM) can provide useful information about D-A blend films, such as their miscibility, distributions, and interpenetrating net structures. To understand the differences in device performance when using different **BDPs** as donors, the morphology of blend film under the optimized condition (D/A weight ratio of 1:0.5) was tested using AFM. Fig. 11 shows the AFM height and phase images of the blend films of the four **BDPs** and PC₆₁BM. The film surface are relatively flat with root-mean-square (RMS) roughness of 0.496 nm for **BDP1**/PC₆₁BM, 0.563 nm for **BDP2**/PC₆₁BM, 0.436 nm for **BDP3**/PC₆₁BM and 0.581 nm for **BDP4**/PC₆₁BM, respectively, and relatively small phase domains are observed in the height images. This indicates that these

BDPs have good miscibility with PC₆₁BM. The phase images in Fig.11 demonstrate that the donor/acceptor interpenetrating network of the blend films of **BDP2** and **BDP4** are better than those of **BDP1/PC₆₁BM** and **BDP3/PC₆₁BM**. In general, good surface morphology would lead to higher exciton dissociation efficiency and thus improve device performance. The good photovoltaic performance of the **BDP2/PC₆₁BM** active layer should be also related to the suitable morphology of the active layer.

4. Conclusions

In summary, a series of novel symmetrical D-A-D structured BODIPY-based dyes, **BDP1-4**, featuring an electron-withdrawing BODIPY motif as the central core, and several types of electron-donating segments, including thiophene, bithiophene, fluorene and carbazole, flanked at its 2,6-positions as terminal groups were successfully synthesized and characterized. These **BDPs** are soluble in common organic solvents, possess panchromatic absorption covering the wavelength range 300–900 nm, and have relatively lower HOMO energy levels of $-5.17 \sim -5.48$ eV. The **BDPs** exhibit excellent thermal stability and good miscibility with PC₆₁BM. **BDP2** show not only good photoelectric characteristic but also superior charge transport property and favorable nanoscale morphology relative to **BDP1**, **BDP3** and **BDP4** and thus pronounce to the higher PCE value of 2.15% under the illumination of AM 1.5G, 100 mW cm⁻² with a V_{oc} of 0.78 V, a J_{sc} of 6.77 mA cm⁻² and FF of 41%. The results indicate that these series of BODIPY based dyes are potential good candidates for the efficient organic solar cell materials. Further engineering of the molecular structure and optimization of the morphology, and variation of the donor moieties, are currently underway in our laboratory in the quest to boost device efficiencies.

Acknowledgements

We greatly acknowledge the financial support from the Nature Science Foundation of Guangdong Province (2014A030313630), the National Nature Science Foundation of China (51476036, 21342003), Project for High-level Personnel of University in Guangdong Province ([2013]246), the Production-Study Research Combinational Project of Guangdong Province and Ministry of Education (2012B091100296), the University Science and Technology Innovation Key Project of Guangdong Province (cxzd1148) and the University and Scientific Research Institution Key Project of Dongguan City (2012108101005).

Appendix A. Supplementary data

Supplementary data related to this article can be found at

References

- [1] Li G, Zhu R, Yang Y. Polymer solar cells. *Nat Photonics* 2012; 6:153-61.
- [2] Cheng YJ, Yang SH, Hsu CS. Synthesis of conjugated polymers for organic solar cell applications. *Chem Rev* 2009;109:5868-923.
- [3] Li Y. Molecular design of photovoltaic materials for polymer solar cells: toward suitable electronic energy levels and broad absorption. *Acc Chem Res* 2012;45:723-33.
- [4] Dou L, You J, Hong Z, Xu Z, Li G, Street RA, Yang Y. 25th Anniversary article: a decade of organic/polymeric photovoltaic research. *Adv Mater* 2013;25:6642-71.
- [5] Lin YZ, Li YF, Zhan XW. Small molecule semiconductors for high-efficiency organic photovoltaics. *Chem Soc Rev* 2012;41:4245-72.
- [6] You JB, Dou LT, Yoshimura K, Kato T, Ohya K, Moriarty T, et al. A polymer tandem solar

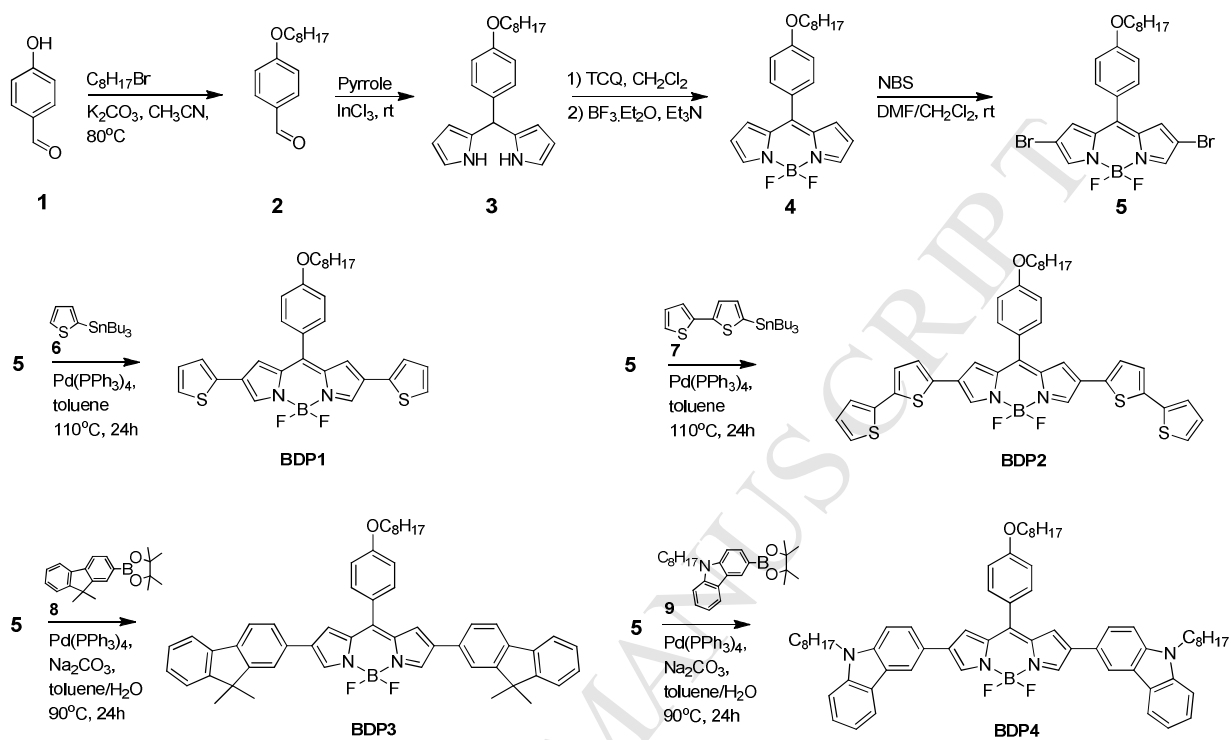
- cell with 10.6% power conversion efficiency. *Nat Commun* 2013;4:1446-55.
- [7] Liu YS, Chen CC, Hong ZR, Gao J, Yang YM, Zhou HP, et al. Solution-processed small-molecule solar cells: breaking the 10% power conversion efficiency. *Sci Rep* 2013;3:3356-63.
- [8] You JB, Chen CC, Hong ZR, Yoshimura K, Ohya K, Xu R, et al. 10.2% power conversion efficiency polymer tandem solar cells consisting of two identical sub-cells. *Adv Mater* 2013;25:3973-8.
- [9] Zhang Q, Kan B, Liu F, Long G, Wan X, Chen X, et al. Small-molecule solar cells with efficiency over 9%. *Nat Photonics* 2014;9:35-41.
- [10] Kan B, Zhang Q, Li M, Wan X, Ni W, Long G, Wang Y, et al. Solution-processed organic solar cells based on dialkylthiol-substituted benzodithiophene unit with efficiency near 10%, *J Am Chem Soc* 2014;136:15529-32.
- [11] Hagfeldt A, Boschloo G, Sun L, Kloo L, Pettersson H. Dye-sensitized solar cells. *Chem Rev* 2010;110:6595-663.
- [12] Marsico F, Turshatov A, Weber K, Wurm FR. A metathesis route for BODIPY labeled polyolefins. *Org Lett* 2013;15:3844-7.
- [13] Ziessel R, Ulrich G, Haefele A, Harriman A. An artificial light-harvesting array constructed from multiple bodipy dyes. *J Am Chem Soc* 2013;135:11330-44.
- [14] Kamkaew A, Lim SH, Lee HB, Kiew LV, Chung LY, Burgess K. BODIPY dyes in photodynamic therapy. *Chem Soc Rev* 2013;42:77-88.
- [15] Kim BS, Ma B, Donuru VR, Liu H, Fréchet JM. Bodipy-backboned polymers as electron donor in bulk heterojunction solar cells. *Chem Commun* 2010;46:4148-50.

- [16] Bura T, Leclerc N, Fall S, Leveque P, Heiser T, Retailleau P, et al. High-performance solution-processed solar cells and ambipolar behavior in organic field-effect transistors with thienyl-BODIPY scaffolds. *J Am Chem Soc* 2012;134:17404-7.
- [17] Bessette A, Hanan GS. Design, synthesis and photophysical studies of dipyrromethene-based materials: insights into their applications in organic photovoltaic devices. *Chem Soc Rev* 2014;43:3342-405.
- [18] Loudet A, Burgess K. BODIPY dyes and their derivatives: syntheses and spectroscopic properties. *Chem Rev* 2007;107:4891-932.
- [19] Donuru VR, Vegnesa GK, Velayudham S, Green S, Liu H. Synthesis and optical properties of red and deep-red emissive polymeric and copolymeric BODIPY dyes. *Chem Mater* 2009;21:2130-8.
- [20] Meng G, Velayudham S, Smith A, Luck R, Liu H. Color tuning of polyfluorene emission with BODIPY monomers. *Macromolecules* 2009;42:1995-2001.
- [21] Wang Y, Chen J, Zhen Y, Jiang H, Yu G, Liu Y, et al. Synthesis and properties of novel near-infrared dye based on BODIPY and diketopyrrolopyrrole units. *Mater Lett* 2015;139:130-3.
- [22] Rousseau T, Cravino A, Bura T, Ulrich G, Ziessel R, Roncali J. BODIPY derivatives as donor materials for bulk heterojunction solar cells. *Chem Commun* 2009;1:673-5.
- [23] Rousseau T, Cravino A, Bura T, Ulrich G, Ziessel R, Roncali J. Multi-donor molecular bulk heterojunction solar cells: improving conversion efficiency by synergistic dye combinations. *J Mater Chem* 2009;19:2298-300.
- [24] Rousseau T, Cravino A, Ripaud E, Leriche P, Rihn S, De Nicola A, et al. A tailored hybrid

- BODIPY-oligothiophene donor for molecular bulk heterojunction solar cells with improved performances. *Chem Commun* 2010;46:5082-4.
- [25] Lin HY, Huang WC, Chen YC, Chou HH, Hsu CY, Lin JT, et al. BODIPY dyes with β -conjugation and their applications for high-efficiency inverted small molecule solar cells. *Chem Commun* 2012;48:8913-5.
- [26] Liu W, Tang A, Chen J, Wu Y, Zhan C, Yao J. Photocurrent enhancement of BODIPY-based solution-processed small-molecule solar cells by dimerization via the meso position. *ACS Appl Mater Interfaces* 2014;6:22496-505.
- [27] Xiao L, Wang H, Gao K, Li L, Liu C, Peng X, et al. A-D-A type small molecules based on boron dipyrromethene for solution-processed organic solar cells. *Chem Asian J* 2015;10:1513-8.
- [28] Zhang X, Zhang Y, Chen L, Xiao Y. Star-shaped carbazole-based BODIPY derivatives with improved hole transportation and near-infrared absorption for small-molecule organic solar cells with high open-circuit voltages. *RSC Adv* 2015;5:32283-9.
- [29] Shimizu S, Iino T, Saeki A, Seki S, Kobayashi N. Rational molecular design towards Vis/NIR absorption and fluorescence by using pyrrolopyrrole aza-BODIPY and its highly conjugated structures for organic photovoltaics. *Chem Eur J* 2015;21:2893-904.
- [30] Mirloup A, Leclerc N, Rihn S, Bura T, Bechara R, Hébraud A, et al. A deep-purple-grey thiophene-benzothiadiazole-thiophene BODIPY dye for solution-processed solar cells. *New J Chem* 2014;38:3644-53.
- [31] Kim YJ, Lee GB, Jeon CW, Kim Y-H, Chung DS, Park CE. A push-pull organic semiconductor with efficient intramolecular charge transfer for solution-processed small

- molecule solar cells. *RSC Adv* 2015;5:3435-42.
- [32] Chen JJ, Conron SM, Erwin P, Dimitriou M, McAlahney K, Thompson ME. High-efficiency BODIPY-based organic photovoltaics. *ACS Appl Mater Interfaces* 2015;7:662-9.
- [33] Cortizo-Lacalle¹ D, Howells CT, Pandey UK, Cameron¹ J, Findlay¹ NJ, Inigo¹ AR, et al. Solution processable diketopyrrolopyrrole (DPP) cored small molecules with BODIPY end groups as novel donors for organic solar cells. *Beilstein J Org Chem* 2014;10:2683-95.
- [34] Liao J, Xu Y, Zhao H, Wang Y, Zhang W, Peng F, et al. Synthesis, optical, electrochemical properties and photovoltaic performance of novel panchromatic meso- thiophene BODIPY dyes with a variety of electron-donating groups at 3,5-positions. *RSC Adv* 2015;5:86453-62.
- [35] Jadhav T, Misra R, Biswas S, Sharma GD. Bulk heterojunction organic solar cells based on carbazole–BODIPY conjugate small molecules as donors with high open circuit voltage. *Phys Chem Chem Phys* 2015;17:26580-8.
- [36] Liao J, Wang Y, Xu Y, Zhao H, Xiao X, Yang X. Synthesis, optical and electrochemical properties of novel meso-triphenylamine-BODIPY dyes with aromatic moieties at 3,5-positions. *Tetrahedron* 2015;71:5078-84.
- [37] Zhao H, Liao J, Ning J, Xie Y, Cao Y, Chen L, et al. Efficient synthesis of novel bis(dipyrromethanes) with versatile linkers via indium(III) chloride-catalyzed condensation of pyrrole and dialdehydes. *Adv Synth Catal* 2010;352:3083-8.
- [38] Duan ZF, Yang ZG, Liu DJ, Cai L, Hoshino D, Morita T, et al. Facile synthesis and characterization of a novel thiophene-fused polycyclic aromatics based on pyrene. *Chin Chem Lett* 2011;22:819-22.
- [39] Liu W, Pink M, Lee, D. Conjugated polymer sensors built on π -extended borasiloxane cages.

- J Am Chem Soc 2009;131:8703-7.
- [40] Li X-C, Liu Y, Liu MS, Jen AK-Y. Synthesis, properties, and application of new luminescent polymers with both hole and electron injection abilities for light-emitting devices. Chem Mater 1999;11:1568-75.
- [41] Axel DB. Density-functional thermochemistry. III. The role of exact exchange. J Chem Phys 1993;98:5648-52.
- [42] Gill PMW, Johnson BG, Pople JA, Frisch MJ. The performance of the Becke-Lee-Yang-Parr (B-LYP) density-functional theory with various basis sets. Chem Phys Lett 1992;197:499-505.
- [43] Frisch MJ, Trucks GW, Schlegel HB, Scuseria GE, Robb MA, Cheeseman JR, et al. Gaussian 09, revision B. 01. Wallingford CT: Gaussian, Inc; 2010.
- [44] Karstens T, Kobs K. Rhodamine B and rhodamine 101 as reference substances for fluorescence quantum yield measurements. J Phys Chem 1980;84:1871-2.
- [45] Zhao H, Wang B, Liao J, Wang H, Tan G. Synthesis, spectral, electrochemical properties, and photovoltaic performance of structurally constrained BODIPY dyes with 4,4'-dimethyl-triphenylamine at the 2,6-positions. Tetrahedron Lett 2013;54:6019-22.
- [46] Malliaras GG, Salem JR, Brock PJ, Scott C. Electrical characteristics and efficiency of single-layer organic light-emitting diodes. Phys Rev B 1998;58:13411-4.
- [47] Fan Q, Li M, Yang P, Liu Y, Xiao M, Wang X, et al. Acceptor-donor-acceptor small molecules containing benzo[1,2-b:4,5-b']dithiophene and rhodamine units for solution processed organic solar cells. Dyes Pigments 2015;116:13-9.



Scheme 1. The synthetic route of **BDP1-4**.

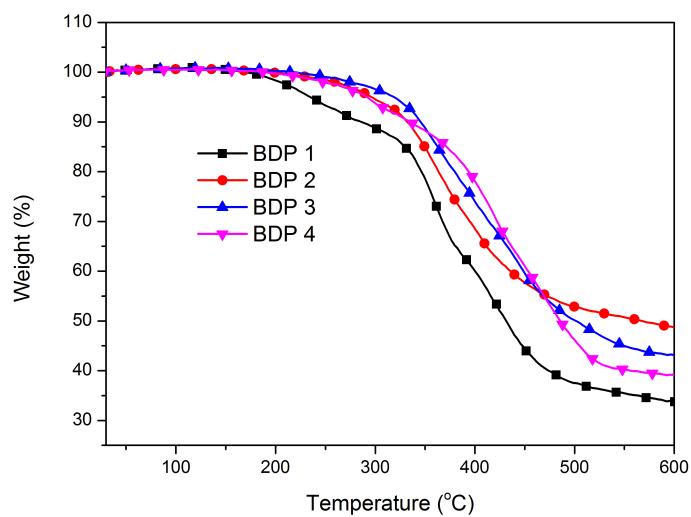


Fig. 1. TGA curves of **BDP1-4** at a heating rate of $20\text{ }^{\circ}\text{C min}^{-1}$ under nitrogen atmosphere.

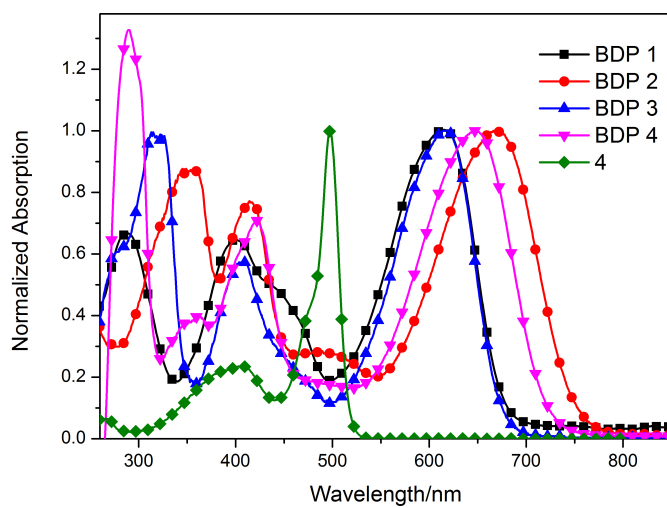


Fig. 2. Normalized absorption spectra of BODIPY 4 and dyes **BDP1-4** in CH_2Cl_2 solution.

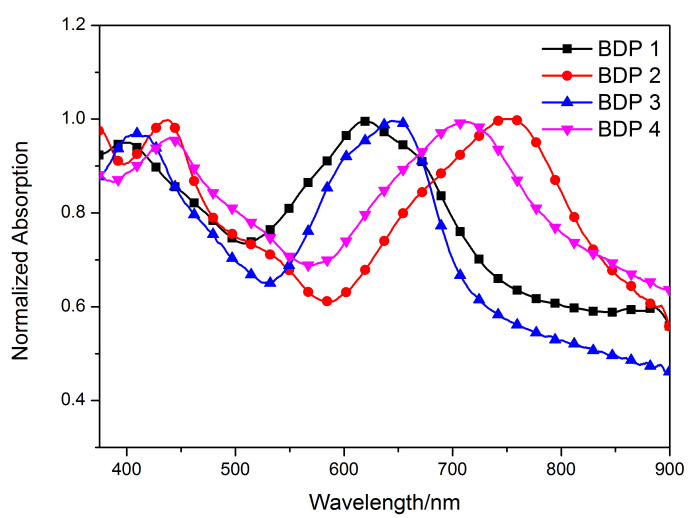


Fig. 3. Normalized absorption spectra of dyes **BDP1-4** in quartz film.

Table 1 Photophysical and thermal properties of **BDP1-4**.

Entries	$\lambda_{\max}^{\text{abs}}$ (nm) ^a	ϵ_{\max} (cm ⁻¹ M ⁻¹)	$\lambda_{\max}^{\text{abs}}$ (nm) ^b	$E_{\text{g}}^{\text{opt}}$ (eV) ^a	$\lambda_{\max}^{\text{em}}$ (nm) ^a	S-S ^c (cm ⁻¹)	Φ_{PL}	T _d (°C)
BDP1	613	0.78 × 10 ⁵	623	1.71	671	1410	0.08	221
BDP2	670	1.13 × 10 ⁵	748	1.59	748	1556	0.02	305
BDP3	616	0.96 × 10 ⁵	647	1.77	668	1263	0.06	328
BDP4	647	1.22 × 10 ⁵	716	1.65	720	1567	0.03	301

^a measured in CH₂Cl₂ solution. ^b measured in the neat film. ^c Stokes shifts.

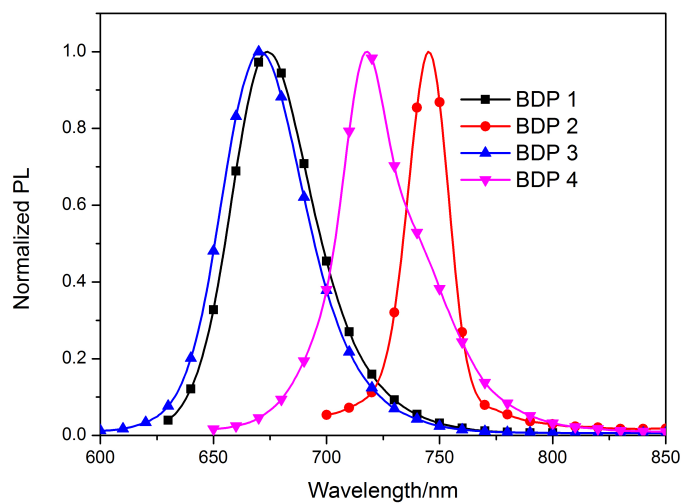


Fig. 4. Normalized fluorescence spectra of **BDP1-4** recorded in CH₂Cl₂ ($c = 1 \times 10^{-7}$ mol/L).

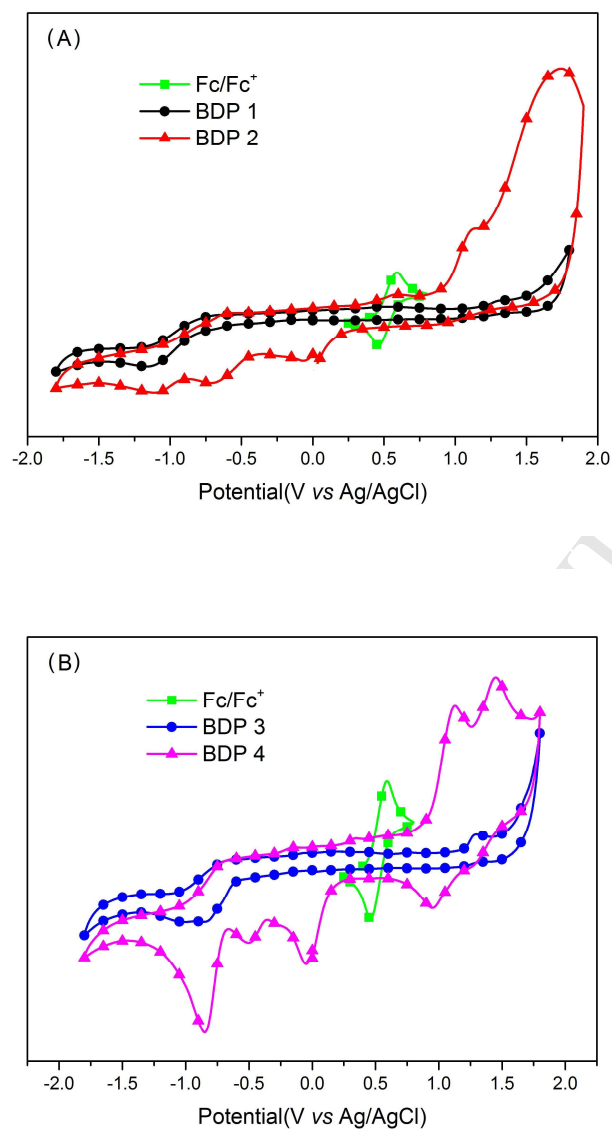


Fig. 5. Cyclic voltammograms of **BDP1-2** (A) and **BDP3-4** (B) in CH_2Cl_2 solution, containing 0.1M $\text{n-Bu}_4\text{NPF}_6$ as the supporting electrolyte recorded at a scan speed of 100 mV/s .

Table 2 Solution electrochemical properties of **BDP1-4**.

Entries	E_g (eV) ^a	$E_{\text{onset}}^{\text{ox}}$ (V) ^b	E_p^{ox} (V) ^c	E_{red} (V) ^d	E_{HOMO} (eV) ^e	E_{LUMO} (eV) ^f
BDP1	1.71	1.15	1.30	-0.56	-5.43	-3.72
BDP2	1.59	0.91	1.15	-0.68	-5.19	-3.60
BDP3	1.77	1.20	1.25	-0.57	-5.48	-3.71
BDP4	1.65	0.89	1.18	-0.76	-5.17	-3.52

^a E_g , estimated from the absorption spectra of dyes absorbed in CH_2Cl_2 solution, $E_g = 1240/\lambda_{\text{onset}}$. ^b $E_{\text{onset}}^{\text{ox}}$, onset

oxidation potential. ^c E_p^{ox} , oxidation peak potential. ^d E_{red} , the reduction potential, was calculated from $E_{\text{onset}}^{\text{ox}} - E_g$.

^e $E_{\text{HOMO}} = [-(E_{\text{onset}}^{\text{ox}} - 0.52) - 4.8]$ eV. ^f $E_{\text{LUMO}} = E_{\text{HOMO}} + E_g$ eV.

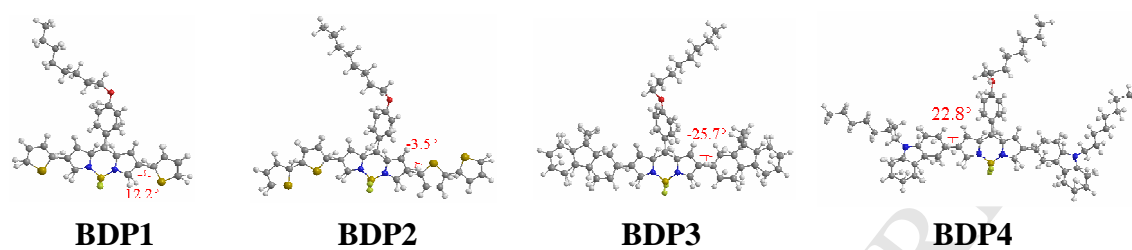


Fig. 6. Optimized structures of **BDP1-4**.

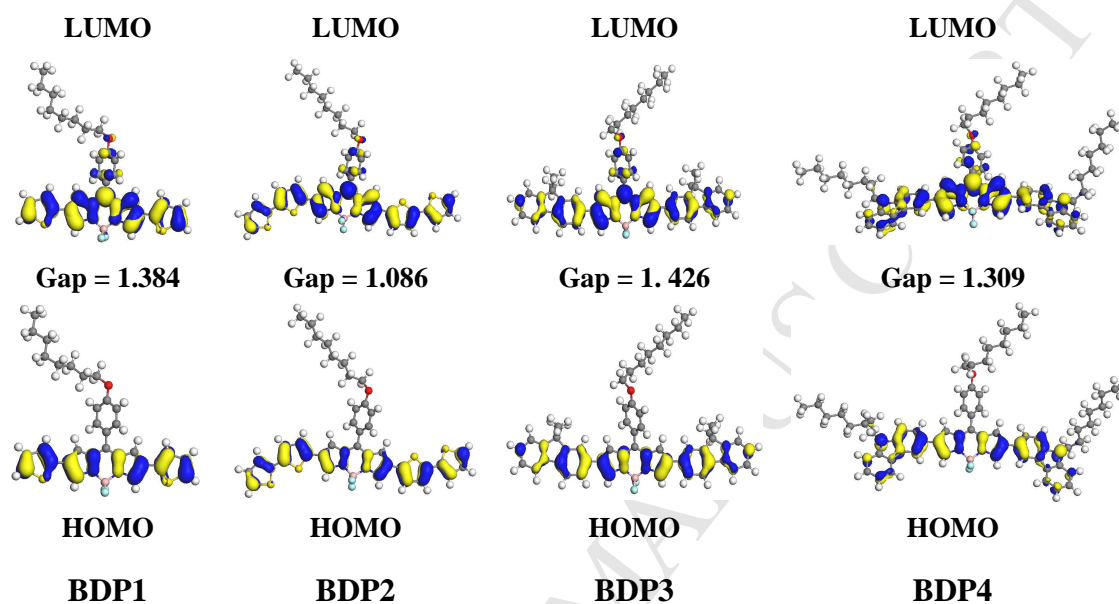


Fig. 7. Electron distribution in HOMO and LUMO levels and energy gaps of **BDP1-4**.

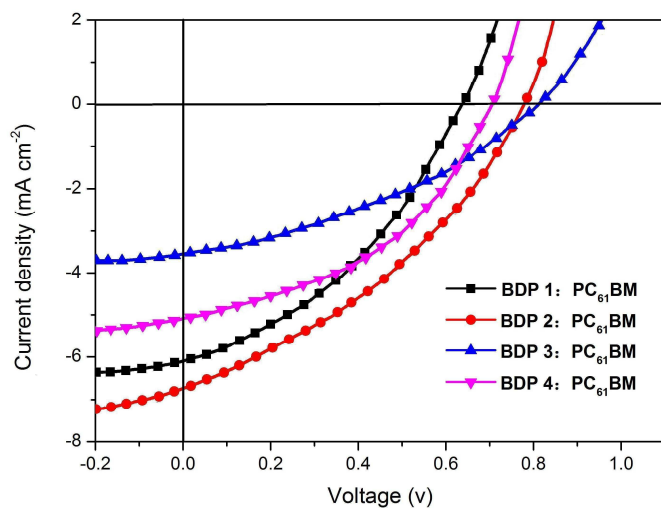


Fig. 8. *J-V* curves of **BDPs/PC₆₁BM**-based OSCs at optimized conditions under the illumination of AM 1.5 G, 100 mW/cm².

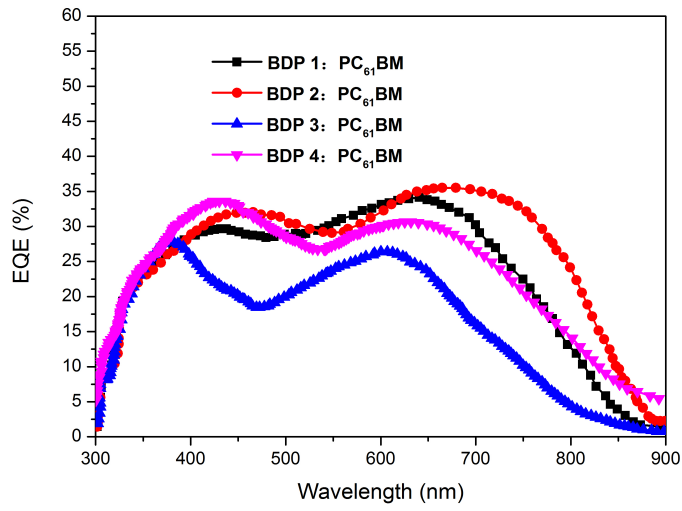


Fig. 9. EQE curves of the optimized **BDPs/PC₆₁BM**-based devices.

Table 3 Photovoltaic performance of OSCs based on the **BDPs**/ PC_{61}BM photoactive layer and the hole mobilities of the **BDPs**/ PC_{61}BM blend films.

Active layers	Ratio (w/w)	V_{oc} (V)	J_{sc} (mA/cm^2)	FF (%)	PCE (%)	Hole mobility ($\text{cm}^2 \text{V}^{-1} \text{s}^{-1}$)
BDP1 : PC_{61}BM	1:0.5	0.64	6.02	39	1.49	8.92×10^{-5}
BDP2 : PC_{61}BM	1:0.5	0.78	6.77	41	2.15	6.35×10^{-4}
BDP3 : PC_{61}BM	1:0.5	0.81	3.62	36	1.06	3.11×10^{-5}
BDP4 : PC_{61}BM	1:0.5	0.70	5.03	44	1.56	6.02×10^{-5}

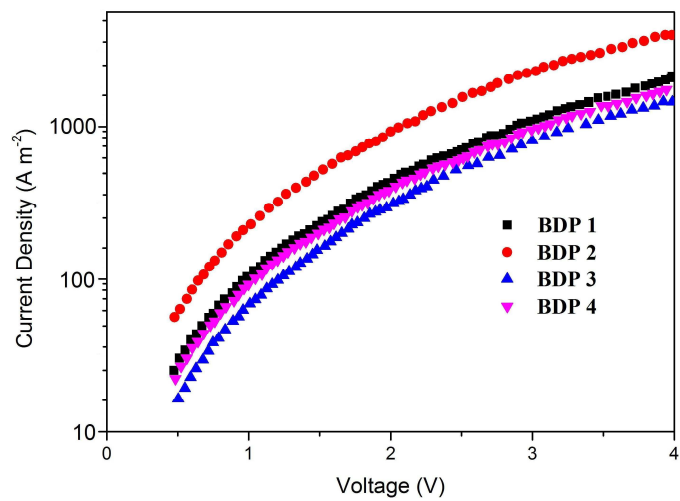


Fig. 10. J - V curves of the optimized hole-only **BDPs** devices.

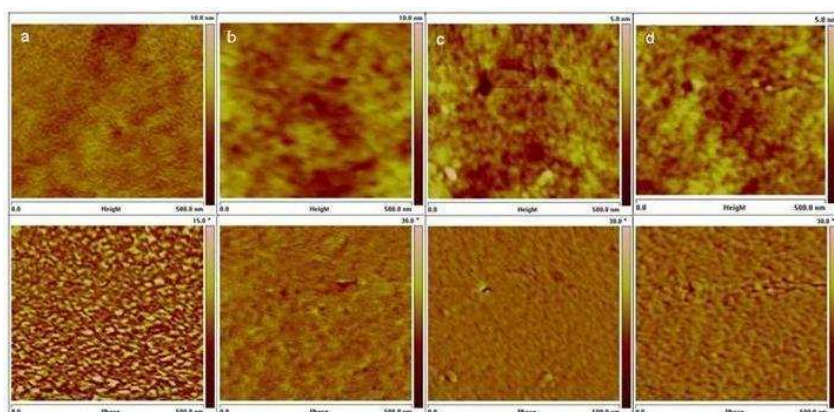


Fig. 11. AFM height images (top) and phase images (bottom) of the blend films of **BDP1**/ PC_{61}BM (a), **BDP2**/ PC_{61}BM (b), **BDP3**/ PC_{61}BM (c), and **BDP4**/ PC_{61}BM (d) with D/A weight ratio of 1:0.5.

Scheme 1. The synthetic route of **BDP1-4**.

Fig. 1. TGA curves of **BDP1-4** at a heating rate of $20\text{ }^{\circ}\text{C min}^{-1}$ under nitrogen atmosphere.

Fig. 2. Normalized absorption spectra of BODIPY **4** and dyes **BDP1-4** in CH_2Cl_2 solution.

Fig. 3. Normalized absorption spectra of dyes **BDP1-4** in quartz film.

Fig. 4. Normalized fluorescence spectra of **BDP1-4** recorded in CH_2Cl_2 ($c = 1 \times 10^{-7}$ mol/L).

Fig. 5. Cyclic voltammograms of **BDP1-2** (A) and **BDP3-4** (B) in CH_2Cl_2 solution, containing 0.1M n-Bu₄NPF₆ as the supporting electrolyte recorded at a scan speed of 100 mV/s.

Fig. 6. Optimized structures of **BDP1-4**.

Fig. 7. Electron distribution in HOMO and LUMO levels and energy gaps of **BDP1-4**.

Fig. 8. *J-V* curves of **BDPs**/PC₆₁BM-based OSCs at optimized conditions under the illumination of AM 1.5 G, 100 mW/cm².

Fig. 9. EQE curves of the optimized **BDPs**/PC₆₁BM-based devices.

Fig. 10. *J-V* curves of the optimized hole-only **BDPs** devices.

Fig. 11. AFM height images (top) and phase images (bottom) of the blend films of **BDP1**/PC₆₁BM (a), **BDP2**/PC₆₁BM (b), **BDP3**/PC₆₁BM (c), and **BDP4**/PC₆₁BM (d) with D/A weight ratio of 1:0.5.

- Novel BODIPY dyes with panchromatic absorption.
- **BDPs** with low ϕ_{FL} and relatively low HOMO levels from -5.17 to -5.48 eV.
- **BDP2/PC₆₁BM** based OSC with PCE of 2.15%.

ACCEPTED MANUSCRIPT